

NMPC-based Cell-Level Thermal Management of EV Batteries in Low Temperature Environment

Wanqun Yang*, Mohammad R. Hajidavalloo**,
Zhaojian Li**, Jun Chen*

* Department of Electrical and Computer Engineering, Oakland
University, Rochester, MI, USA

Emails: {wanqunyang, junchen}@oakland.edu

** Department of Mechanical Engineering, Michigan State University,
East Lansing, MI, USA

Emails: {hajidava, lizhaoj1}@msu.edu

Abstract: One of the main reasons electric vehicles (EVs) struggle to completely replace fuel-powered cars is their limited driving range, which can be significantly reduced during extreme cold environment. Existing study on battery thermal management often treats EV batteries as a singular unit and ignores the thermal gradient among battery cells. To overcome this issue, a nonlinear model predictive control (NMPC)-based optimal strategy for cell-level thermal management of EV batteries is proposed. The considered thermal management system consists of a heat pump to warm up coolant fluid, three-way valves to divert coolant between different cell branches, and a flow-reversible pump to change coolant direction in real-time. A mixed-integer optimization problem is then formulated, where the integer variable corresponds to the flow direction and the continuous variables include heat pump compressor speed, flow speed, and coolant flow distributions among different cell branches. Compared to non-flow-reversible thermal management system, simulation results suggest that the proposed system can reduce the cell thermal gradient by 16.6% throughout the simulation and by 42.1% during steady state.

Keywords: Model predictive control, electric vehicles, thermal management.

1. INTRODUCTION

Electric vehicles (EVs) have come into people's view due to their environmental and economical friendliness in most regions. However, EV development has reached a bottleneck, making it difficult to fully replace fuel-powered vehicles (Khaleel et al. (2024)). For instance, current EVs still require a long charging time to achieve a limited driving range (Feng et al. (2025)). Moreover, EVs also face drawbacks such as a reduced range at cold temperatures and potential battery safety risks at high temperatures (Xie et al. (2022); Senol et al. (2023); Chen et al. (April 7–9, 2021); Zhang et al. (2022b)).

Specifically, in low temperature environments, there are several limitations concerning discharging EV batteries. Firstly, for current Li-ion batteries, a low temperature environment slows down the diffusion speed of Li ions within the electrolyte and electrodes (Zhang et al. (2022a)), limiting the discharging capacity of the battery pack which in turn affects EV driving range. Secondly, under low temperature conditions, the initial resistance of the battery increases, causing a voltage drop (Shidore and Bohn (2008)) and increasing Ohmic heat losses, both of which can decrease the output power of the battery. Finally, the battery can experience significantly higher capacity

loss during at low temperatures, due to the accelerated formation of lithium plating.

To address these challenges related to low temperatures, an increasing number of researchers are focusing on thermal management systems. For instance, Guo et al. (2023) take into account both cabin space and seat heating, with control objectives primarily aimed at balancing energy consumption and driver comfort, and Hajidavalloo et al. (2023) utilize a heat pump for battery and cabin heating due to the higher thermal efficiency. In terms of control methods, Liu et al. (2023); Cen and Jiang (2020) demonstrate the use of PID control, while Xie et al. (2023); Park and Kim (2019) apply control with neural networks. Advanced control methods such as MPC have been studied by Hajidavalloo et al. (2023). Although these works cover most aspects of the thermal management systems required for EVs, the battery pack is typically considered as a singular unit when transferring heat with the coolant. In reality, as the coolant flows through the battery pack loop, its temperature changes significantly, creating significant thermal gradient among battery cells, which needs to be minimized to preserve battery life.

To overcome this issue, this paper proposes an NMPC-based cell-level battery thermal management system (BTMS). Specifically, detailed thermal dynamics of each cell and its heat transfer with coolant fluid are explic-

¹ This work is supported in part by National Science Foundation through Award #2237317. *Corresponding author: J. Chen.*

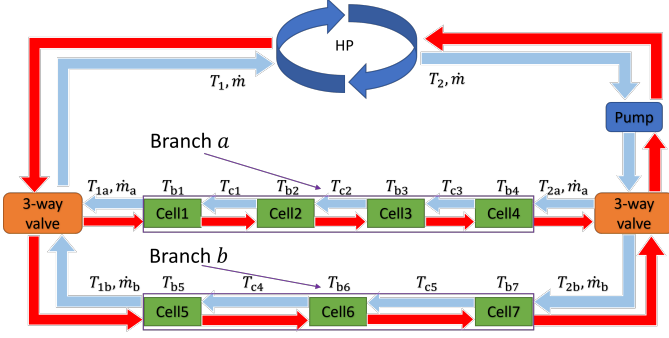


Fig. 1. Battery thermal management system under study. Red: counterclockwise flow direction; Blue: clockwise flow direction.

itly modeled and considered in the control design. Additionally, to reduce thermal gradient among battery cells, a flow-reversible pump is incorporated into the system. Moreover, a mixed-integer optimization problem is formulated, where the integer variable corresponds to the flow direction and the continuous variables include heat pump compressor speed, flow speed, and coolant flow distributions among different cell branches. Similar to (Hajidavalloo et al. (2023)), for any given coolant flow direction, an NMPC-based optimal strategy is used to control the continuous variables (compressor speed, flow speed, and flow distributions). Our simulation results show that compared to non-flow-reversible pump BTMS, our proposed system can significantly reduce the standard deviation of battery cells temperature. The contributions of this paper are summarized as follows.

- (1) A detailed cell-level battery thermal model is developed, in which cells are (electrically) connected in series to provide traction power for the EV.
- (2) A coolant system is designed to provide heat to battery while reducing thermal gradient among cells, featuring the capability to reverse the coolant flow direction for more effective thermal management of each cell.
- (3) An NMPC-based control strategy has been designed to control the continuous variables, which ensures that the battery cells can reach and maintain the target temperature as fast as possible.

The remainder of this paper is organized as follows. Section 2 introduces the proposed cell-level BTMS along with its models, while the NMPC problem and its stage cost function are discussed in Section 3. Simulation results and discussions are presented in Section 4, and Section 5 concludes the paper with future work directions.

2. DESIGN & MODELING

Fig. 1 plots the system proposed in the paper, where the battery pack is divided into seven cell groups. A heat pump is used to warm up the coolant fluid and three-way valves are used to divert coolant between two cell branches. To achieve more uniform temperature control without excessively increasing system complexity, the coolant loop is designed with two branches, heating four battery cells and three battery cells respectively. After heating the battery cells, the coolant merges and flows back into the heat pump. Additionally, the coolant loop is designed to

Table 1. Notations for the proposed BTMS with reversible coolant flow

Notation	Physical meaning	unit
T_1, T_2	coolant temp. after or before HP	$^{\circ}C$
T_{1a}, T_{2a}	coolant temp. at the inlet or outlet of coolant Branch a	$^{\circ}C$
T_{1b}, T_{2b}	coolant temp. at the inlet or outlet of coolant Branch b	$^{\circ}C$
$T_{c1} - T_{c5}$	5 coolant temp. within the branch	$^{\circ}C$
$T_{b1} - T_{b7}$	7 battery cells temp.	$^{\circ}C$
\dot{m}_a	battery Branch a coolant flow rate	kg/s
\dot{m}_b	battery Branch b coolant flow rate	kg/s
\dot{m}	total coolant flow rate	kg/s
n_{comp}	compressor speed	rpm

allow the flow direction reversal. In Fig. 1, the red arrows denote the counterclockwise coolant flow direction and the blue arrows denote the clockwise coolant direction.

The following subsection introduces more details about the models of the heat pump, flow pump, and electrothermal behavior of the battery. To improve the readability of the paper, the counterclockwise coolant flow direction, which is marked in red in Fig. 1, is used to explain the system and reference equations. A brief summary at the end of this section will describe the impacts to the models with clockwise flow direction. Table 1 list the nomenclature used in this paper.

2.1 Flow Pump Model

Based on Fig. 1, the flow pump is located after the three-way valve, and the coolant mixing temperatures can be determined as

$$\dot{m} = \dot{m}_a + \dot{m}_b, \quad (1a)$$

$$T_1 = \frac{1}{\dot{m}} (\dot{m}_a T_{1a} + \dot{m}_b T_{1b}), \quad (1b)$$

$$T_2 = \frac{1}{\dot{m}} (\dot{m}_a T_{2a} + \dot{m}_b T_{2b}). \quad (1c)$$

The pump power can be modeled as

$$P_{pump} = \frac{P_{pump,m}}{\eta_m} = \frac{1}{\eta_m} \cdot \frac{\Delta p_{pump} \dot{m}}{\rho_c}, \quad (2)$$

where $P_{pump,m}$ represents the pump power, η_m denotes the power conversion rate of the pump, ρ_c is the coolant density, and Δp_{pump} is the pressure drop of the pump can be calculated based on the mass flow rate as follows, according to (Ma et al. (2022)),

$$\Delta p_{pump} = 0.927 \dot{m}^2 + 0.586 \dot{m} - 0.143. \quad (3)$$

2.2 Heat Pump Model

In Cvok et al. (2021)'s works, the coefficient of performance (COP) of the heat pump (HP) has been tested to reach values between 2.5 and 3.0 even in cold environments, such as $-10^{\circ}C$. Therefore, HP is used to heat the coolant instead of a positive temperature coefficient heater, whose maximum COP is about 1 (Zhang et al. (2023)). Fig. 1 shows that after the coolant from the two branches merges at the lower temperature T_2 , it is heated by HP to T_1 and then enters the branches through the three-way valve. The governing equation is given by

$$C\dot{T}_1 = \dot{Q}_{HP} + \dot{m}c_c(T_2 - T_1), \quad (4)$$

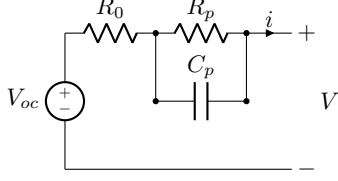


Fig. 2. The first-order ECM circuit for a battery cell.

where c_c is the heat capacity of the coolant. In this paper, G-48 ethylene-glycol is chosen as the coolant, which is a highly popular choice in the EV industry (Kalaf et al. (2021)). C denotes the thermal inertia of the coolant and is equal to the product of the coolant mass m and the c_c in the loop.

Finally, \dot{Q}_{HP} is the heat transfer rate of HP, which can be calculated based on its COP and power as follows.

$$\dot{Q}_{HP}(T_{amb}, n_{comp}) = COP_{HP}(T_{amb}, n_{comp}) \cdot P_{HP}, \quad (5)$$

where P_{HP} is the power of HP, primarily affected by the compressor speed n_{comp} , and is selected as an additional control variable. More details about the performance of HP under different temperatures, and the relationships between COP, heat capacity, and compressor speed, can be found in (Liu et al. (2018)).

2.3 Electrothermal Battery Model

Equivalent circuit model (ECM) has been extensively studied for analyzing battery electrothermal behaviors (Chen et al. (2024); Lin et al. (2014); Chen et al. (2022)). This paper adopts the first-order ECM for each battery cell as shown in Fig. 2, where V_{oc} represents the cell's open-circuit voltage when no power load is applied and is related to the cell state of charge (SOC). R_o denotes the ohmic resistance, which is the internal resistance of the battery cell. R_p and C_p represent the polarization resistance and polarization capacitance, respectively. i is the discharge current, and V_p is the polarization voltage across R_p , which can be modeled as

$$\dot{V}_p = -\frac{V_p}{R_p C_p} + \frac{i}{C_p}. \quad (6)$$

Here we use the convention that a positive value of i denotes discharging and a negative value of i denotes charging. And the terminal voltage V of the battery pack is:

$$V = V_{oc} - iR_o - V_p. \quad (7)$$

Note that the value of V_{oc} is based on cell SOC, and R_o , R_p , and C_p are all related to both the temperature and SOC of the battery cell. Therefore, (6) and (7) are nonlinear. The dynamic of SOC is expressed as

$$\dot{SOC}_{cell,i} = -\frac{i}{3600 \times C_{cell}}, \quad (8)$$

where C_{cell} denotes the cell capacity in Ah. In this paper, the battery pack is assumed to consist of seven cells with the same initial SOC, connected in series as the power source for the EV. Note that the connection in Fig. 1 represents the connection of coolant loop, while the electrical connections are not explicitly depicted in Fig. 1.

In modeling the heat exchange process of the battery pack, the seven battery cells are assumed to have the same

specific heat capacity c_b and mass m_b , and the thermal inertia of a single battery cell is given by $C_b = c_b m_b$. As shown in Fig. 1, after being heated by the HP, the coolant has a flow rate \dot{m} with a temperature T_1 . After passing through the three-way valve, the coolant enters Branch a with a flow rate \dot{m}_a and a temperature T_{1a} , and enters Branch b with a flow rate \dot{m}_b and a temperature T_{1b} , where $T_{1a} = T_{1b}$ at system startup. After flowing through the two branches, the coolant fluid has two outlet temperatures, T_{2a} and T_{2b} , which mix to form the temperature T_2 before entering the HP.

Taking Branch a as an illustration, the differential equations for battery cells 1, 2, 3, and 4 are:

$$C_b \dot{T}_{b1} = R_{b1} i^2 + \dot{m}_a c_c (T_{1a} - T_{c1}) - h_{a1} (T_{b1} - T_a), \quad (9a)$$

$$C_b \dot{T}_{b2} = R_{b2} i^2 + \dot{m}_a c_c (T_{c1} - T_{c2}) - h_{a2} (T_{b2} - T_a), \quad (9b)$$

$$C_b \dot{T}_{b3} = R_{b3} i^2 + \dot{m}_a c_c (T_{c2} - T_{c3}) - h_{a2} (T_{b3} - T_a), \quad (9c)$$

$$C_b \dot{T}_{b4} = R_{b4} i^2 + \dot{m}_a c_c (T_{c3} - T_{2a}) - h_{a1} (T_{b4} - T_a). \quad (9d)$$

The first term on the right side of equations (9a)–(9d) represents the internal resistance heat generation of the battery cells, while the second term accounts for the heat gain from the coolant, and the last term represents the heat lost to the ambient air. Here, T_a is the ambient temperature, and h_{ai} denotes the heat transfer coefficient between the ambient air and the battery cell i . The difference between h_{a1} and h_{a2} is that the former is used for the first and last battery cells within a branch, while the latter is applied to the middle battery cells. Moreover, h_{a1} is chosen to be greater than h_{a2} to account for the middle cells' reduced surface area in contact with the ambient air.

Furthermore, based on the energy balance within the system, the governing equations for the coolant temperatures in Branch a and at the outlet are given by

$$C_2 \dot{T}_{c1} = \dot{m}_a c_c (T_{1a} - T_{c1}) - h_b (T_{c1} - T_{b1}), \quad (10a)$$

$$C_2 \dot{T}_{c2} = \dot{m}_a c_c (T_{c1} - T_{c2}) - h_b (T_{c2} - T_{b2}), \quad (10b)$$

$$C_2 \dot{T}_{c3} = \dot{m}_a c_c (T_{c2} - T_{c3}) - h_b (T_{c3} - T_{b3}), \quad (10c)$$

$$C_2 \dot{T}_{2a} = \dot{m}_a c_c (T_{c3} - T_{2a}) - h_b (T_{2a} - T_{b4}), \quad (10d)$$

where $C_2 = m_{clnt,a} c_c$ is the thermal inertia of the coolant in Branch a , and $m_{clnt,a}$ is the mass of coolant surrounding the battery cells. On the right side of equations (10a)–(10d), the first term represents the energy balance of the coolant, and the second term corresponds to the heat loss of the coolant when it transfers heat to the battery cells. Here, h_b is the heat transfer coefficient based on the contact surface area with the battery cells. Specifically, T_{2a} in equation (10d) represents the temperature of the outlet coolant. Lastly, in Fig. 1, the inlet coolant temperatures are T_{1a} and T_{1b} , which are modeled in (1) and (4).

2.4 System Model with Clockwise Coolant Flow

The blue arrows in Fig. 1 indicate that the coolant flows clockwise. In this case, the coolant enters Branch a with a flow rate \dot{m}_a and a temperature T_{2a} , and enters Branch b with a flow rate \dot{m}_b and a temperature T_{2b} . Similar to the counterclockwise flow direction, the two outlet coolant streams then mix, forming a flow rate \dot{m} and a temperature T_1 before entering the HP. Consequently, for the HP model, the differential equations for T_1 and T_2 are similar to (4) and are given by

$$C\dot{T}_2 = \dot{Q}_{HP} + \dot{m}c_c(T_1 - T_2). \quad (11)$$

Moreover, the governing equations for the battery cells' temperatures will also change. Taking Branch a as an illustration, the differential equations for cell temperatures, similar to (9), are given by

$$C_b\dot{T}_{b1} = R_{b1}i^2 + \dot{m}_a c_c(T_{c1} - T_{1a}) - h_{a1}(T_{b1} - T_a), \quad (12a)$$

$$C_b\dot{T}_{b2} = R_{b2}i^2 + \dot{m}_a c_c(T_{c2} - T_{c1}) - h_{a2}(T_{b2} - T_a), \quad (12b)$$

$$C_b\dot{T}_{b3} = R_{b3}i^2 + \dot{m}_a c_c(T_{c3} - T_{c2}) - h_{a2}(T_{b3} - T_a), \quad (12c)$$

$$C_b\dot{T}_{b4} = R_{b4}i^2 + \dot{m}_a c_c(T_{2a} - T_{c3}) - h_{a1}(T_{b4} - T_a). \quad (12d)$$

And the coolant temperatures in Branch a , similar to (10), are given by

$$C_2\dot{T}_{c1} = \dot{m}_a c_c(T_{c2} - T_{c1}) - h_b(T_{c1} - T_{b2}), \quad (13a)$$

$$C_2\dot{T}_{c2} = \dot{m}_a c_c(T_{c3} - T_{c2}) - h_b(T_{c2} - T_{b3}), \quad (13b)$$

$$C_2\dot{T}_{c3} = \dot{m}_a c_c(T_{2a} - T_{c2}) - h_b(T_{c3} - T_{b4}), \quad (13c)$$

$$C_2\dot{T}_{1a} = \dot{m}_a c_c(T_{c1} - T_{1a}) - h_b(T_{1a} - T_{b1}). \quad (13d)$$

It is worth mentioning that the inlet coolant temperatures in the counterclockwise flow are T_{2a} and T_{2b} , which are modeled in (1) and (11), respectively.

3. NMPC FORMULATION

In this section, an NMPC problem is formulated to find the optimal control actions for the proposed BTMS. Recall that the differential equations for describing the nonlinear system dynamic are given in Section 2, which can be compactly represented as

$$\dot{x} = f_c(x, u) \quad (14)$$

and the state vector x and control input vector u are defined as follows

$$x = [SOC_{(b_1-b_7)}, T_{(b_1-b_7)}, T_{(c_1-c_5)}, T_{1a}, T_{1b}, T_{2a}, T_{2b}]^T,$$

$$u = [\dot{m}_a, \dot{m}_b, n_{comp}]^T.$$

where $SOC_{(b_1-b_7)}$ denotes the seven SOC values of the seven battery cells, $T_{(b_1-b_7)}$ represents the temperatures of the seven battery cells, and $T_{(c_1-c_5)}$ corresponds to the five coolant temperatures within the branches. Moreover, the finite receding-horizon optimal control problem (OCP) at each time step is given as follows

$$\min_{\mathbf{u}} J(x_0, \mathbf{u}) = \sum_{k=0}^{N-1} l(\mathbf{x}(k), \mathbf{u}(k)), \quad (15a)$$

$$\text{s.t. } \mathbf{x}(0) = \mathbf{x}_0, \mathbf{x}(k+1) = f_d(\mathbf{x}(k), \mathbf{u}(k)), \quad (15b)$$

$$x_{\min} \leq \mathbf{x}(k) \leq x_{\max}, k = 0, \dots, N, \quad (15c)$$

$$g_{\min} \leq g(\mathbf{u}(k)) \leq g_{\max}, k = 0, \dots, N-1. \quad (15d)$$

In the above OCP, N is the prediction horizon, and x_0 represents the initial state of the dynamic system. $f_d(\mathbf{x}(k), \mathbf{u}(k))$ is the discretized version of $f_c(x, u)$ with a sampling time of T_s . x_{\min} and x_{\max} are the lower and upper bound values, given as follows

$$x_{\min} = [0_{(b_1-b_7)}, T_{a(b_1-b_7)}, T_{a(c_1-c_5)}, T_a, T_a, T_a, T_a]^T, \quad (16)$$

$$x_{\max} = [1_{(b_1-b_7)}, 35_{(b_1-b_7)}, 70_{(c_1-c_5)}, 70, 70, 70, 70]^T.$$

Recall that $T_{a(b_1-b_7)}$ represents the temperatures of the seven battery cells, which are initially set to the ambient temperature T_a at the beginning of the state. For the input constraints (15d), $g(u)$ is given by

$$g(u) = [u(1), u(2), u(3), u(1) + u(2), u(1) - u(2)]^T. \quad (17)$$

Algorithm 1 NMPC-Based BTMS Algorithm

Parameters: Initial State x_0 , NMPC prediction horizon N , MIP sampling time T_d

```

1:  $c \leftarrow 0$ ;
2:  $d^* \leftarrow 0$ ;
3: for each time step  $k$  do
4:    $c \leftarrow c + 1$ ;
5:   if  $c = T_d$  then
6:      $(\mathbf{u}_0^*, J_0^*) \leftarrow$  Solve NMPC 15 with initial state
        $x_k$  and  $d = 0$ ;
7:      $(\mathbf{u}_1^*, J_1^*) \leftarrow$  Solve NMPC 15 with initial state
        $x_k$  and  $d = 1$ ;
8:     if  $J_0^* \leq J_1^*$  then
9:        $d^* \leftarrow 0, \mathbf{u}^* \leftarrow \mathbf{u}_0^*$ ;
10:    else
11:       $d^* \leftarrow 1, \mathbf{u}^* \leftarrow \mathbf{u}_1^*$ ;
12:    end if
13:     $c \leftarrow 0$ ;
14:    else
15:       $\mathbf{u}^* \leftarrow$  Solve NMPC 15 with  $d = d^*$ ;
16:    end if
17:     $u_k \leftarrow \mathbf{u}^*(1)$ ;
18:     $x_{k+1} \leftarrow f(x_k, u_k)$  as Equ. (14);
19: end for

```

and g_{\min} and g_{\max} are given by

$$g_{\min} = [0, 0, 0, 0, -0.02]^T, g_{\max} = [0.1, 0.1, 0.1, 4000, 0.02]^T.$$

Note that the constraint related to $u(1) - u(2)$ is used to balance the flow rates between two branches to avoid excessive differences.

The stage cost function l in (15a) is given by:

$$l(x, u) = \sum_{i=1}^{n=7} \alpha_1 (T_{bi} - T_{\text{target}})^2 + \alpha_2 (P_{Pump} + P_{HP}), \quad (18)$$

where T_{target} is the optimal operating temperature of the battery cells. The first term of (18) penalizes the deviation of cell temperature from the target. The second term of (18) penalizes the power consumption of the flow pump and heat pump. Note that α_1 and α_2 are the weights of the two terms, respectively, to balance battery cell heating and power consumption.

The proposed BTMS algorithm is shown in Algorithm 1.

4. SIMULATION RESULTS

For simulation, α_1 and α_2 for the NMPC stage cost function (18) are set to 6000 and 1, respectively, and T_{target} is set to 10°C . Moreover, the ambient temperature is assumed to range between -15°C and -5°C and follows a normal distribution, all the simulations use same temperature distribution data. Likewise, we assume that the vehicle moves in ideal conditions with constant resistance and that the battery pack supplies a constant output current throughout. The NMPC prediction horizon is set to $N = 25$ and sampling time is set to $T_s = 4$.

Three case studies are performed for the proposed BTMS system. In Case I and Case II, we set $T_d = T_s$ and $T_d = 40T_s$, which optimize flow direction for each time step and every 40 time steps, respectively. In Case III, the coolant flow direction is forced to change every 40 time steps. To demonstrate the performance of the proposed system,

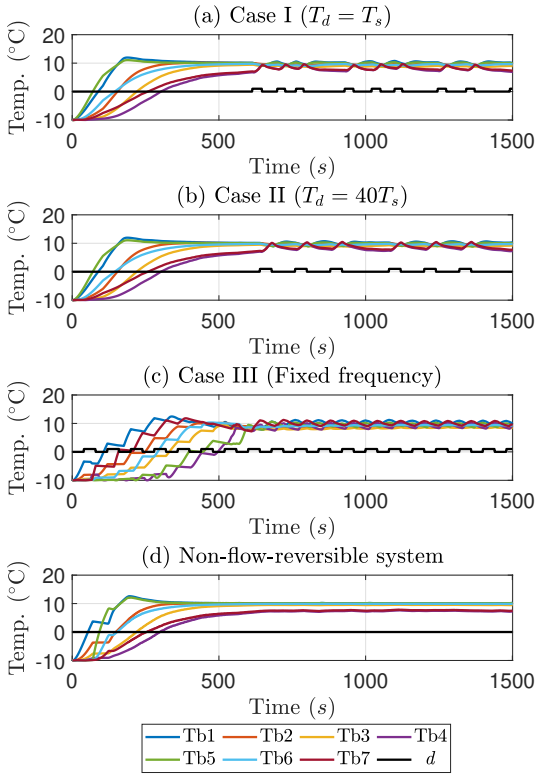


Fig. 3. Comparison of battery cell temperatures.

a non-flow-reversible pump system is also simulated and compared. Note that in the non-flow-reversible system, all the components remain the same as in the proposed BTMS except that the flow direction does not change, which is assumed to be counterclockwise for simulation.

Fig. 3 plots the simulation results. The black line with values of 0 and 1 represents the flow direction at the current time step, with 0 indicating counterclockwise flow and 1 clockwise flow. For the proposed BTMS, as shown in Fig. 3(a)-(c), the cell temperatures vary when the coolant flow direction changes, while the average temperature remain close to the target temperature. As comparison, for the non-flow-reversible system, as shown in Fig. 3(d), the temperatures of the last battery cells in the two branches, i.e., T_{b4} and T_{b7} , deviate significantly from the T_{target} .

Table 2 lists key metrics for performance analysis. In this table, T_{ss} refers to the 7% settling time, i.e., time step at which the average temperature reaches 9.3°C for the first time, σ_{tr} denotes the standard deviation of the cell temperature before the average cell temperature reaches the steady temperature, while σ_{ss} represents the standard deviation of the cell temperature after the average cell temperature reaches the target. Finally, σ_{all} denotes the standard deviation of the cell temperature throughout the whole simulation. For all three σ metrics, a lower value indicates less thermal gradients among the seven battery cells in this phase. It can be observed that the battery cells in the non-flow-reversible pump system fail to reach the steady temperature at 9.3°C , demonstrating the impact of temperature deviations in the later battery cells on the overall battery pack. Therefore, in this case,

Table 2. Comparison of standard deviation of cell temperature

Methods	T_{ss}	σ_{tr}	σ_{ss}	σ_{all}
Case I ($T_d = T_s$)	645	3.540	0.833	1.997
Case II ($T_d = 40T_s$)	669	3.463	0.724	1.946
Case III (Fixed frequency)	720	4.016	0.800	2.344
Non-flow-reversible	∞	3.960	1.250	2.334

we calculate σ_{tr} and σ_{ss} using the cell temperatures before and after time step 600. Moreover, Fig. 4 shows the average temperature and standard deviation of cell temperatures with respect to time, where Fig. 4(b) is the standard deviation over the whole simulation and Fig. 4(c) focuses on phase after T_{ss} .

When $T_d = T_s$, the average cell temperature can reach the steady temperature in 645 seconds, a significant improvement compared to the case of without direction changes. This demonstrates the importance of flow direction control in the proposed BTMS. However, as mentioned before, optimizing flow direction with $T_d = T_s$ requires computing two NMPC solutions at every time step, significantly increasing the computational demand. Therefore, an alternative setting of $T_d = 40T_s$ is tested, where two NMPC costs J_0^* and J_1^* are compared every 40 time steps. As shown in Table 2, by increasing T_d , T_{ss} increases slightly (compared to Case I), resulting in a slower warming process. On the other hand, this is compensated by a smoother temperature distribution among cells. In addition, Fig. 4(b) and (c) reveal that the standard deviations differ significantly for different approaches. In particular, Case II demonstrates a 42.1% reduction in σ_{all} compared to the case of non-flow-reversible pump system. Fig. 4(c) shows that the standard deviation in the Case II is lower than non-flow-reversible system at each time step. Case II achieve lowest standard deviation in all phases. Finally, for Case III with fixed frequency, i.e., no optimization is performed for the flow direction, Fig. 4(b) indicates that the standard deviation remains relatively high before T_{ss} , rather than gradually smoothing out as in the other cases. It can also be seen in Table 2 that the standard deviation is significantly higher than Case I and Case II. Those results demonstrate the presence of a higher thermal gradient in Case III.

5. CONCLUSIONS

This paper proposed a nonlinear model predictive control (NMPC)-based optimal strategy for cell-level battery thermal management in electric vehicles (EVs). The proposed system integrates a heat pump for coolant heating, three-way valves for flow distribution, and a flow-reversible pump to enhance temperature uniformity among battery cells. A mixed-integer optimization approach was utilized to determine the optimal control inputs, where the integer variable corresponds to the flow direction and the continuous variables include heat pump compressor speed, flow speed, and coolant flow distributions among different cell branches. Simulation results demonstrate the advantages of the proposed system over the non-flow-reversible pump system, achieving a 16.6% reduction in overall temperature variation and a 42.1% reduction at steady state. These findings confirm that incorporating flow direction control into BTMS significantly enhances thermal uni-

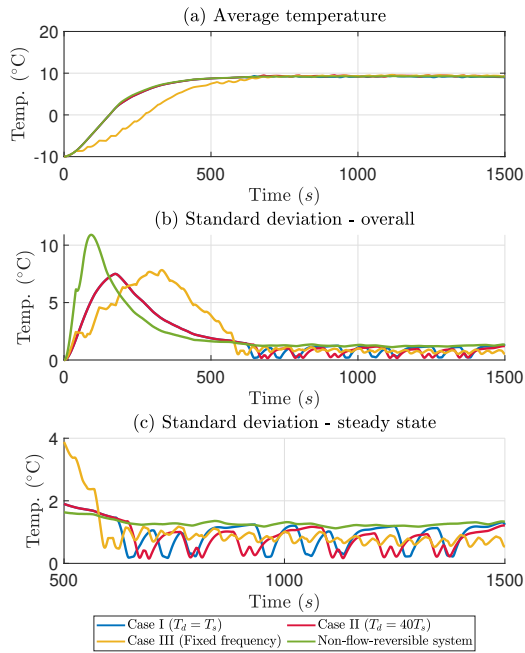


Fig. 4. Comparison of average temperature and temperature variations with respect to time.

formity, thereby improving battery performance in cold environments. Future work will focus on incorporating the flow-direction decision directly into the MPC formulation and scaling the approach to include more cells, extending the proposed approach to dynamic driving conditions, and validating the strategy through real-world experiments to further optimize EV battery thermal management.

REFERENCES

- Cen, J. and Jiang, F. (2020). Li-ion power battery temperature control by a battery thermal management and vehicle cabin air conditioning integrated system. *Energy for Sustainable Development*, 57, 141–148.
- Chen, J., Behal, A., and Li, C. (2024). Active battery cell balancing by real time model predictive control for extending electric vehicle driving range. *IEEE Trans. Auto. Sci. Eng.*, 21(3), 4003–4015.
- Chen, J., Liang, M., and Ma, X. (April 7–9, 2021). Probabilistic analysis of electric vehicle energy consumption using MPC speed control and nonlinear battery model. In *IEEE Green Technologies Conference*. Denver, CO.
- Chen, J., Zhou, Z., Zhou, Z., Wang, X., and Liaw, B. (2022). Impact of battery cell imbalance on electric vehicle range. *Green Energy and Intelligent Transportation*, 1(3), 100025.
- Cvok, I., Škugor, B., and Deur, J. (2021). Control trajectory optimisation and optimal control of an electric vehicle hvac system for favourable efficiency and thermal comfort. *Optimization and Engineering*, 22(1), 83–102.
- Feng, J., Liu, W., and Chen, F. (2025). Moving towards a circular economy: A systematic review of barriers to electric vehicle battery recycling. *Sustainable Production and Consumption*.
- Guo, R., Li, L., Sun, Z., and Xue, X. (2023). An integrated thermal management strategy for cabin and battery heating in range-extended electric vehicles under low-temperature conditions. *Applied Thermal Engineering*, 228, 120502.
- Hajidavalloo, M.R., Chen, J., Hu, Q., Song, Z., Yin, X., and Li, Z. (2023). Nmpc-based integrated thermal management of battery and cabin for electric vehicles in cold weather conditions. *IEEE Transactions on Intelligent Vehicles*, 8(9), 4208–4222.
- Kalaf, O., Solyali, D., Asmael, M., Zeeshan, Q., Safaei, B., and Askir, A. (2021). Experimental and simulation study of liquid coolant battery thermal management system for electric vehicles: A review. *International journal of energy research*, 45(5), 6495–6517.
- Khaleel, M., Nassar, Y., El-Khozondar, H.J., Elmnifi, M., Rajab, Z., Yaghoubi, E., and Yaghoubi, E. (2024). Electric vehicles in china, europe, and the united states: Current trend and market comparison. *Int. J. Electr. Eng. and Sustain.*, 1–20.
- Lin, X., Perez, H.E., Mohan, S., Siegel, J.B., Stefanopoulou, A.G., Ding, Y., and Castanier, M.P. (2014). A lumped-parameter electro-thermal model for cylindrical batteries. *Journal of Power Sources*, 257, 1–11.
- Liu, C., Zhang, Y., Gao, T., Shi, J., Chen, J., Wang, T., and Pan, L. (2018). Performance evaluation of propane heat pump system for electric vehicle in cold climate. *International Journal of Refrigeration*, 95, 51–60.
- Liu, Z., Liu, Z., Liu, J., and Wang, N. (2023). Thermal management with fast temperature convergence based on optimized fuzzy pid algorithm for electric vehicle battery. *Applied Energy*, 352, 121936.
- Ma, Y., Ding, H., Liu, Y., and Gao, J. (2022). Battery thermal management of intelligent-connected electric vehicles at low temperature based on nmpc. *Energy*, 244, 122571.
- Park, J. and Kim, Y. (2019). Supervised-learning-based optimal thermal management in an electric vehicle. *IEEE Access*, 8, 1290–1302.
- Senol, M., Bayram, I.S., Naderi, Y., and Galloway, S. (2023). Electric vehicles under low temperatures: A review on battery performance, charging needs, and power grid impacts. *Ieee Access*, 11, 39879–39912.
- Shidore, N. and Bohn, T. (2008). Evaluation of cold temperature performance of the jcs-vl41m phev battery using battery hil. *Electric and Hybrid-Electric Vehicles–Batteries*, 133.
- Xie, J., Yang, R., Gooi, H.B., and Nguyen, H.D. (2023). Pid-based cnn-lstm for accuracy-boosted virtual sensor in battery thermal management system. *Applied Energy*, 331, 120424.
- Xie, P., Jin, L., Qiao, G., Lin, C., Barreneche, C., and Ding, Y. (2022). Thermal energy storage for electric vehicles at low temperatures: Concepts, systems, devices and materials. *Renewable and Sustainable Energy Reviews*, 160, 112263.
- Zhang, N., Deng, T., Zhang, S., Wang, C., Chen, L., Wang, C., and Fan, X. (2022a). Critical review on low-temperature li-ion/metal batteries. *Advanced Materials*, 34(15), 2107899.
- Zhang, N., Lu, Y., Kadam, S., and Yu, Z. (2023). Investigation of the integrated fuel cell, battery, and heat pump energy systems. *Energy Conversion and Management*, 276, 116503.
- Zhang, X., Li, Z., Luo, L., Fan, Y., and Du, Z. (2022b). A review on thermal management of lithium-ion batteries for electric vehicles. *Energy*, 238, 121652.